LETTER

https://doi.org/10.1038/s41586-019-0940-x

Rolling of the jaw is essential for mammalian chewing and tribosphenic molar function

Bhart-Anjan S. Bhullar[1,2,6]*, Armita R. Manafzadeh[3,6], Juri A. Miyamae[1,2], Eva A. Hoffman[4,5], Elizabeth L. Brainerd[3], Catherine Musinsky[5] & Alfred W. Crompton[5]

Over the past two centuries, mammalian chewing and related anatomical features have been among the most discussed of all vertebrate evolutionary innovations[1–3]. Chief among these features are two characters: the dentary-only mandible, and the tribosphenic molar with its triangulated upper cusps and lower talonid basin[3–5]. The flexible mandibular joint and the unfused symphysis of ancestral mammals—in combination with transformations of the adductor musculature and palate—are thought to have permitted greater mobility of each lower jaw, or hemimandible[6,7]. Following the appearance of precise dental occlusion near the origin of the mammalian crown[8,9], therians evolved a tribosphenic molar with a craggy topography that is presumed to have been used to catch, cut and crush food. Here we describe the ancestral tribosphenic therian chewing stroke, as conserved in the short-tailed opossum *Monodelphis domestica*: it is a simple symmetrical sequence of lower tooth-row eversion and inversion during jaw opening and closing, respectively, enacted by hemimandibular long-axis rotation. This sequence is coupled with an eversion–inversion rotational grinding stroke. We infer that the ancestral therian chewing stroke relied heavily on long-axis rotation, including symmetrical eversion and inversion (inherited from the first mammaliaforms) as well as a mortar-and-pestle rotational grinding stroke that was inherited from stem therians along with the tribosphenic molar. The yaw-dominated masticatory cycle of primates, ungulates and other bunodont therians is derived; it is necessitated by a secondarily fused jaw symphysis, and permitted by the reduction of high, interlocking cusps[10–12]. The development of an efficient masticatory system—culminating in the tribosphenic apparatus—allowed early mammals to begin the process of digestion by shearing and crushing food into small boli instead of swallowing larger pieces in the reptilian manner, which necessitates a long, slow and wholly chemical breakdown. The vast diversity of mammalian teeth has emerged from the basic tribosphenic groundplan[13].

Only a handful of previous studies have included direct observations of feeding in mammals that retain the ancestral tribosphenic dentition (Fig. 1). Of these studies, only two (on the Virginia opossum, *Didelphis virginiana*) have used X-ray imagery to record the mechanics of the chewing stroke[10,14,15]. But when restricted to two dimensions, even X-ray images cannot adequately capture the complexity of jaw movement—especially long-axis rotation, which may have been instrumental in the attainment of precise mammalian occlusion[16]. Current hypotheses about the nature of long-axis rotation in tribosphenic mammals rely on toothwear, which suggests inversion of the tooth row before occlusion[17], and on a preliminary single-trial 2D fluoroscopic study of one *Didelphis* opossum[10]. In this latter study, the authors observed asymmetry between the 'working side' and the neutral 'balancing side'

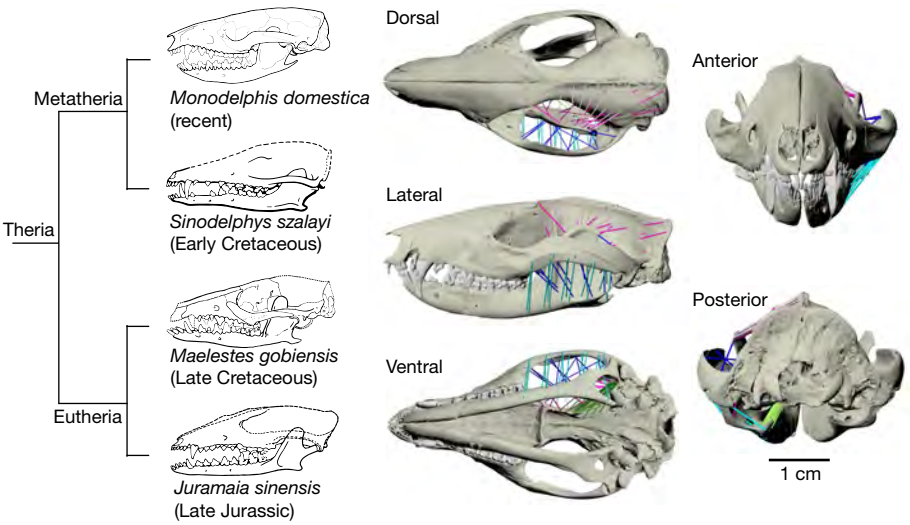

Fig. 1 | Conservation of ancestral therian features in the skull of *Monodelphis*. The skull of *Monodelphis* retains the ancestral therian groundplan and is similar to those of early stem marsupials (Metatheria) and placentals (Eutheria) in being small, long-snouted and endowed with a full set of high-crowned tribosphenic molars. Skulls have been redrawn and modified from the following references: *Monodelphis* from ref. [23], *Sinodelphys* from ref. [24], *Maelestes* from ref. [13], and *Juramaia* from ref. [26]. The 3D reconstruction from the μCT scan includes reconstructed muscles. Cyan, superficial masseter; dark blue, deep masseter; light pink, superficial temporalis; dark pink, deep temporalis; dark green, lateral pterygoid; light green, medial pterygoid. The relative phylogenetic positions of taxa are shown following previous work[26].

[1]Department of Geology & Geophysics, Yale University, New Haven, CT, USA. [2]Peabody Museum of Natural History, Yale University, New Haven, CT, USA. [3]Department of Ecology and Evolutionary Biology, Brown University, Providence, RI, USA. [4]Department of Geology, Jackson School of Geosciences, The University of Texas at Austin, Austin, TX, USA. [5]Museum of Comparative Zoology, Harvard University, Cambridge, MA, USA. [6]These authors contributed equally: Bhart-Anjan S. Bhullar, Armita R. Manafzadeh. *e-mail: bhart-anjan.bhullar@yale.edu

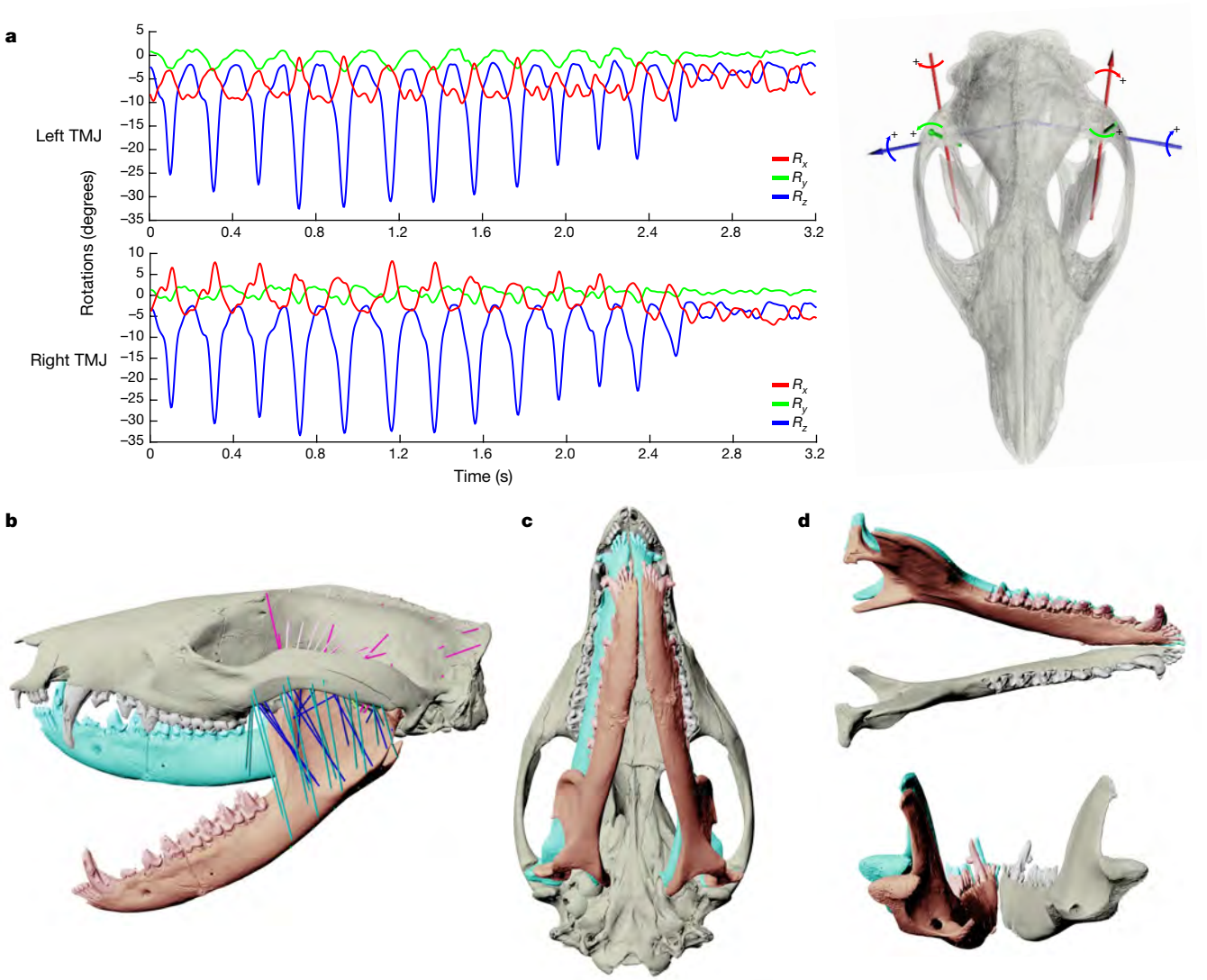

Fig. 2 | Summary of temporomandibular joint kinematics. a, In the left panels, the left (working side) and right (balancing side) temporomandibular joint (TMJ) rotations for a typical chewing sequence are shown in the top and bottom panels, respectively (from an individual opossum eating wax worms; representative of six total trials from two opossums). In the right panel, the joint coordinate systems are shown on a cranium in dorsal view. The plus signs indicate conventions for positive rotations. **b**, Extremes of gape (*z* axis rotation), relative to a fixed cranium. **c**, Extremes of yaw (*y* axis rotation), relative to a fixed cranium. **d**, Extremes of roll (that is, hemimandibular long-axis rotation; *x* axis rotation), relative to a fixed right hemimandible.

of the jaw; both the working and balancing sides everted during jaw opening, but during jaw closing they observed inversion of the working side and continued eversion of the balancing side.

No direct observations of the occlusal phase of chewing are possible using 2D fluoroscopy, because the teeth are hidden when the jaw is nearing closure. Moreover, reconstructions of tooth operation have relied upon an idealized upper and lower molar pair, without considering variation along the tooth row. Previous authors have compared the lower talonid basin and the upper protocone to a mortar and pestle, which implies that back-and-forth grinding accompanies the in-and-out chewing stroke[18]. However, inferences based on toothwear and on the manipulation of physical and digital models have yielded the hypothesis that a simple inversion–eversion chewing stroke occurs without grinding[19].

We undertook a marker-based X-ray reconstruction of moving morphology (XROMM)[20] investigation of chewing in the short-tailed opossum *M. domestica* to visualize skeletal kinematics and augmented these kinematic data with muscle reconstructions based on contrast-enhanced micro-computed tomography (μCT), using a recently described method[21] (Fig. 1). Didelphimorpha is the sister taxon of most or all other marsupials. Aside from the inflected angle of the jaw shared with other marsupials (which may be related to ear ontogeny, and has previously been stated to have little effect on masticatory function[22]), didelphids largely retain the ancestral therian jaw configuration, including an unfused symphysis and tribosphenic dentition[23]. Their craniodental morphology is widely considered to resemble that of the therian ancestor[24–26] (Fig. 1). In a test of this common assumption, we performed a geometric morphometric analysis that demonstrated that the opossum jaw is similar in shape to both the therian and to the common mammalian ancestor (Extended Data Figs. 1–3, Supplementary Information). It lies near in shape-space to the Jurassic mammaliaforms *Morganucodon*, *Docodon* and *Hadrocodium* (Extended Data Fig. 1). There is no plesiomorphic early-diverging clade of placental mammals comparable to Didelphidae: the basal split in placentals (which is as-yet unresolved) involves the three highly derived clades Afrotheria, Xenarthra and Boreoeutheria[27]. To our knowledge, the only previous XROMM study on mammalian feeding used miniature pigs, which represent derived artiodactyls that have highly modified jaw morphology that includes low-crowned bunodont dentition, a fused symphysis and an unusual bilateral chewing sequence[16]. This study reported extensive yaw of the fused mandible, and little to no roll.

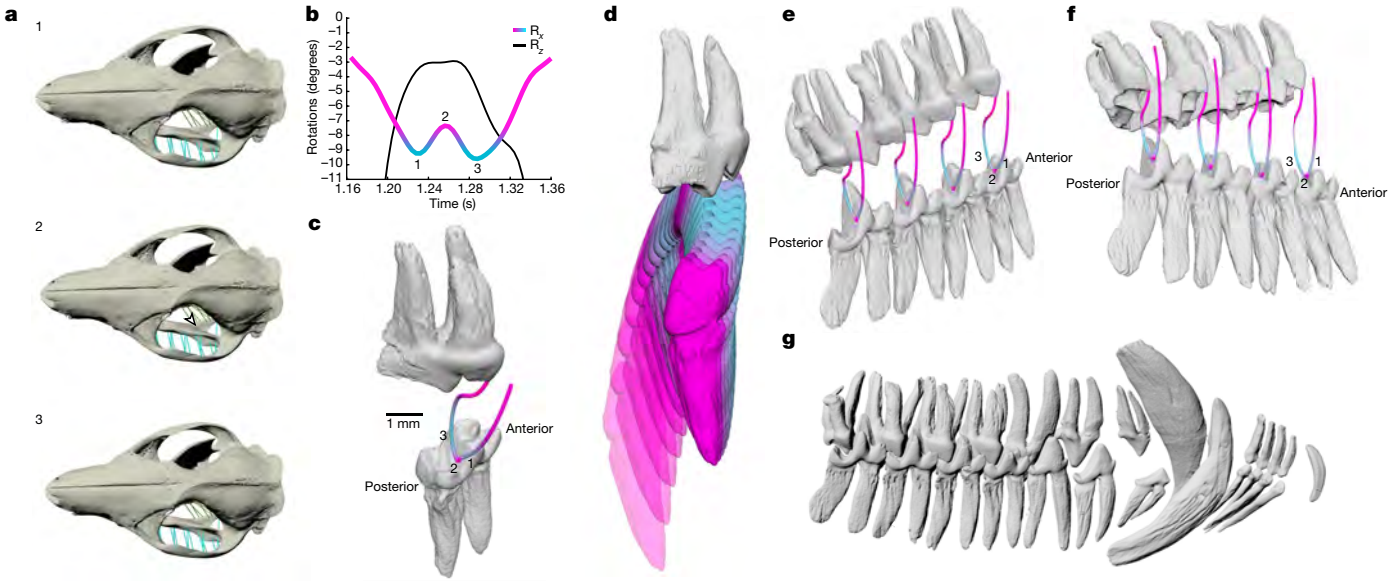

Fig. 3 | The rotational grinding stroke and occlusion along the tooth row. a, Dorsal view of the cranium, highlighting the attachments of the superficial masseter (cyan) and medial pterygoid (light green). Note the appearance and disappearance of the mandibular foramen (indicated by the arrowhead in (2)) caused by hemimandibular roll. See also Supplementary Video 3. **b**, Working side gape (*z* axis rotation) and roll (*x* axis rotation), coloured by hemimandibular long-axis rotation. Magenta is more externally rotated and cyan is more internally rotated, during maximum occlusion (representative of 152 total rotational grinding strokes from 2 opossums). **c**, Path of the protocone of the first upper molar, relative to a fixed lower molar during a chew sequence. **d**, Path of the lower first molar relative to a fixed upper molar during a chewing sequence. See also Supplementary Video 6. Colouring conventions in **c** and **d** match those in **b**. Three homologous time points (1, 2 and 3) are marked in **a**–**c**. **e**, **f**, Paths of the protocones of the four left molars in posteromedial (**e**) and ventromedial (**f**) view. The time points (1, 2 and 3) are homologous with those in **a**–**c**. See also Supplementary Video 5. **g**, Maximum occlusion along the entire left tooth row, shown in medial view.

The degree to which the motions of mastication are stereotyped was immediately evident from our trials. Among all trials, and despite expected variation, patterns of jaw movement were similar in sequence and overall form, regardless of food type (Fig. 2, Extended Data Figs. 4–7, Supplementary Videos 1, 2; see Extended Data Fig. 7 and Supplementary Information for discussion of temporomandibular joint translations). During hard-food trials, teeth remained more separated, which is in keeping with the larger size of the kibble used in these trials as opposed to the mealworms used in soft-food trials (Extended Data Fig. 6). As expected, we observed independent movement of the hemimandibles (Extended Data Figs. 6, 8). Occlusion was unilateral with occasional side-switches. Gape—or *z* axis rotation in our temporomandibular joint coordinate system (Fig. 2a)—was simple, rhythmic and symmetrical, including swift closure of the jaw until contact with food (fast-close phase), a slow-close masticatory phase and slow opening (Fig. 2a, b). The major jaw adductor muscles, especially the masseter and temporalis, shortened during closure as expected[10] (Fig. 2, Extended Data Figs. 4, 9). Yaw–or *y* axis rotation—served largely to bring the lower teeth, which in resting position are inset from the upper, into alignment on the working side, and was a fairly minor component of jaw movement despite previous work that suggests otherwise[28] (Fig. 2a, c). By contrast, there was considerable hemimandibular long-axis rotation (*x* axis rotation or roll) (Fig. 2a, d, Extended Data Fig. 6).

In all experimental trials, long-axis rotation was broadly symmetrical, in contrast to the distinct asymmetry that has previously been reported[10]. At rest, the hemimandibles were somewhat everted, or splayed, such that the tooth rows faced outward and the lower canines were outside the upper canines. During jaw opening, the hemimandibles rolled further outward (that is, their upper edges everted); during closing, they rolled symmetrically inward (or towards the vertical), which brought the lower teeth into position for interlocking occlusion with the upper teeth (Fig. 2a). Closing and inversion both slowed as the teeth engaged food within the mouth.

During maximum closure, we observed an eversion–inversion sequence that—to our knowledge—has not previously been described; here, we call this sequence the rotational grinding stroke (Fig. 3). This quick, but important, movement was near-ubiquitous in complete chews and traversed up to 90% of average per-stroke *x* axis rotation (Supplementary Table 1), drawing the central depression of the lower talonid basins transversely across the upper protocones (Extended Data Fig. 5e, f). Changes in the relative positions of reconstructed muscle attachments indicated a shortening of the superficial masseter and the medial pterygoid during inversion and eversion, respectively (Fig. 3a, Extended Data Fig. 9, Supplementary Video 3), as was suggested by previously published preliminary electromyography data[10]. We propose that the unexpectedly simple and roughly symmetrical pattern of (1) jaw opening paired with eversion, (2) jaw closing paired with inversion and (3) the rotational grinding stroke are plesiomorphic features of therian chewing.

We were able to observe occlusion in detail by following the trajectories of individual tooth pairs along the entire tooth row. Although the general fit of molars was as predicted from toothwear and models[19], we found that, contrary to previous hypotheses[15], inversion and eversion continued during the slow-close and slow-open phases of chewing (during which food is processed), which resulted in additional transverse movement of the teeth relative to each other. In addition, the rotational grinding stroke (that is, back-and-forth jaw roll at greatest jaw closure) enacted a reverse mortar-and-pestle action of the talonid basin 'mortar' against the protocone 'pestle', which represents a notable addition to the traditional approach-and-departure model of molar interaction[19,29] (Fig. 3b–f, Supplementary Videos 4–6). Previous studies[5,15] have used an idealized molar pair to demonstrate hypotheses regarding occlusion, whereas here we individually examined each tooth position and found broadly similar molar occlusal patterns along the tooth row (Fig. 3e, f, Supplementary Video 5). The posterior two premolars—which are large enough to occlude, but the interactions of which have never been addressed using in vivo functional studies—approached each other closely in a simple edge-to-edge slicing stroke, with greatest alignment at maximum jaw inversion (Fig. 3g). The first premolar and canines did not closely approach each other during chewing.

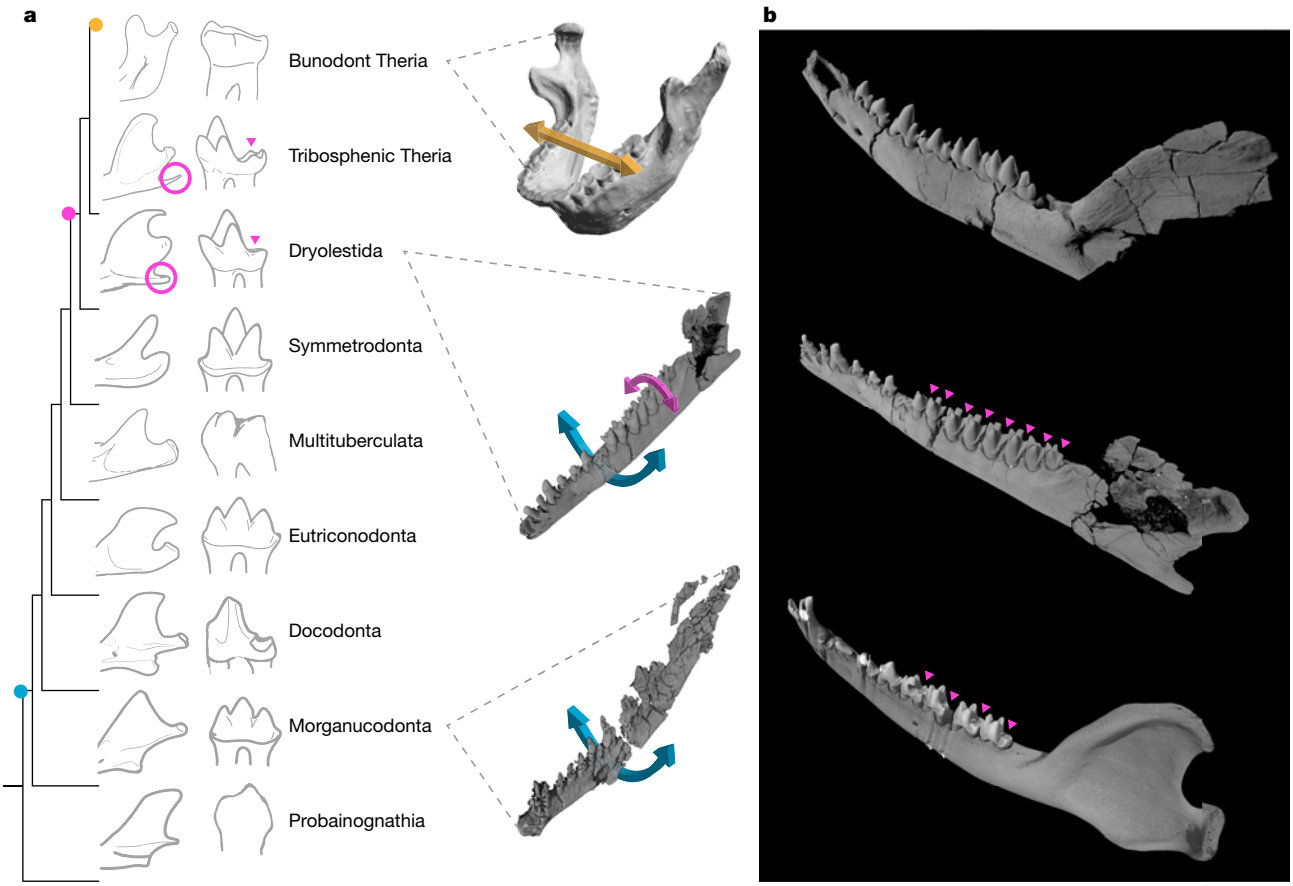

Fig. 4 | Evolution of mammalian jaw morphology and kinematics. **a**, Relationships of major clades on the stem and in the crown of Mammalia, with drawings of the back of the jaw in medial view (left) and molar teeth in lingual view (right). We infer that simple long-axis rotation appeared at Mammaliaformes (blue dot on tree, blue curved arrow on μCT scan images of jaws to far right). The rotational grinding stroke appeared at Cladotheria (pink dot, pink curved arrow), in concert with the angular process (circled) and the talonid basin (pink arrowhead). Some derived therians (orange dot on tree) have lost the ability to perform hemimandibular rotation by fusing the symphysis and diminishing the angular process. Typically, they process food using jaw yaw (orange arrow), which is possible owing to their low rounded (bunodont) tooth cusps. Images were redrawn and modified from sources listed in the Supplementary Information and ref. [28]. **b**, Origin of the talonid basin. Eutriconodonts (top) have simple tricuspid teeth similar to those those of primitive cynodonts. Dryolestoids (middle) have small talonid 'shelves' that presage the larger talonid basins of therian mammals (bottom). The relative phylogenetic positions of taxa are shown following previous work[28,33].

Here we present an in vivo 3D kinematic analysis of the nature of chewing in a conservative therian mammal. Our two core observations are (1) that the hemimandibles symmetrically evert their tooth rows by rolling outward along their long axes during jaw opening, and invert by rolling inward during jaw closing, and (2) that at the deepest part of the bite, the mandibles evert then invert, which further processes the food in the rotational grinding stroke. We posit that each of these kinematic patterns arose at a crucial time during mammalian evolution: the jaw roll evolving in concert with precise occlusion just before the origin of Mammalia, and the rotational grinding stroke evolving in concert with the talonid basin of the tribosphenic molar before the origin of Theria (Fig. 4a).

Unlike their cynodont ancestors, mammaliaforms have lower jaws that are everted or tilted outward at rest, possibly owing to early embryonic effects of brain expansion on the temporomandibular region[30–32]. Precise unilateral occlusion would have been impossible without inverting the lower teeth, and evidence from wear facets indicates that hemimandibular long-axis rotation appeared crownward of *Sinoconodon* and stemward of *Morganucodon*[8,9] (Fig. 4a). Determinate growth and limited dental replacement, both of which serve to maintain tooth alignment, appeared contemporaneously with rotation. Because long-axis rotation was in evidence early during mammaliaform evolution, and because wear-based indicators of rotation persist along the mammalian stem, inversion and eversion of the hemimandibles in opossums are most parsimoniously interpreted as having been retained from the original mammaliaform chewing sequence. Functionally relevant regions of the dentary are notably conserved: the dentary symphysis and condyle of *Monodelphis* are broadly similar to those of *Morganucodon*[23] (Extended Data Fig. 3), although the therian glenoid more tightly grips the condyle than in Morganucodonta, as is the overall shape of the mandible (Extended Data Figs. 1, 2). Indeed, the majority of non-molar tooth-row morphology is fairly unchanged from Morganucodonta to Theria: incisors, canines and premolars remain largely consistent in form and, presumably, function[26]. Preliminary data from goats[10] have been interpreted as showing the same basic pattern of inversion and eversion, and we note that jaw action in monotremes (specifically, echidnas) has also previously been described[32] as the product of symmetrical hemimandibular eversion and inversion. Therefore, we hypothesize that the overall kinematics of the opossum jaw during opening and closing, and the operation of the premolars in particular, are direct retentions from ancestral triconodont mammaliaforms.

We tentatively suggest that the rotational grinding stroke originated with the talonid shelf of Cladotheria (Fig. 4b). The fact that the therian angular process appeared concurrently with the talonid shelf is probably not a coincidence[28] (Fig. 4a, b). Development of the angular process increases the mechanical advantage of both the external masseter and the medial pterygoid by dropping their insertions well below the central axis of the jaw, and increasing their area of attachment. As confirmed by

our dynamic reconstructions, these two muscles are principally responsible for rolling the jaw. We also note that in the early mammaliaforms *Morganucodon* and *Dinnetherium* a 'pseudangular process' is present alongside wear-based evidence for considerable long-axis rotation, and that in various docodonts and australosphenidans—all of which have a 'pseudotribosphenic' tooth morphology—the process is particularly well-developed[8,33]. It is possible that docodonts and australosphenidans even had some form of rotational grinding stroke, whether or not this was homologous to that of tribosphenic mammals. By contrast, eutriconodontans, multituberculates and some early symmetrodontans had reduced angular processes. We tentatively hypothesize that jaw roll was secondarily reduced in these taxa.

Recent work has emphasized the importance of jaw yaw in producing medial movement during occlusion in cladotherians, partly on the basis of previous studies that have asserted that roll was minimal in these taxa[28]; we propose that, although mandibular yaw is important in positioning the tooth row, hemimandibular roll is the principal mechanism of grinding in Cladotheria. According to our hypothesis, yaw-driven grinding (in the sense of considerable side-to-side motion) originated as a derived condition well within the therian crown—for instance, in various ungulate clades and in primates (Fig. 4a). Each time yaw-driven grinding evolved, it was accompanied by symphysial fusion that prevented long-axis rotation, and a flattening of the tooth cusps (bunodonty) that released the upper and lower dentition from mutual entrapment[10,11,13]. In each of these cases, the angular process disappeared as hemimandibular rotation was rendered impossible.

By permitting precise occlusion and efficient food processing, jaw roll is likely to have supported a high metabolic rate and large brain in ancestral mammals. The rotational grinding stroke and the tribosphenic molar were added to the initial simple kinematic pattern and triconodont dentition, which were central to therian dominion and the rise of mammals.

Online content

Any methods, additional references, Nature Research reporting summaries, source data, statements of data availability and associated accession codes are available at https://doi.org/10.1038/s41586-019-0940-x.

Received: 4 August 2018; Accepted: 18 January 2019;
Published online 13 February 2019.

1. Hunter, J. *The Natural History of the Human Teeth: Explaining Their Structure, Use, Formation, Growth, and Diseases* (J. Johnson, London, 1778).
2. Owen, R. *On the Anatomy of Vertebrates, Vol. II. Birds and Mammals* (Longmans, Green and Co., London, 1866).
3. Crompton, A. W. The origin of the tribosphenic molar. In *Early Mammals: 2. Symposium Arranged by the Linnean Soc.* (ed. Kermack, D. M.) 65–87 (Linnean Society of London, London, 1971).
4. Crompton, A. W. & Hylander, W. L. in *The Ecology and Biology of Mammal-like Reptiles* (ed. Hotton, N.) 263–282 (Smithsonian Institution Press, Washington DC, 1986).
5. Crompton, A. W. & Hiiemäe, K. Functional occlusion in tribosphenic molars. *Nature* **222**, 678–679 (1969).
6. Crompton, A. W. & Parker, P. Evolution of the mammalian masticatory apparatus. *Am. Sci.* **66**, 192–201 (1978).
7. Oron, U. & Crompton, A. W. A cineradiographic and electromyographic study of mastication in *Tenrec ecaudatus*. *J. Morphol.* **185**, 155–182 (1985).
8. Jenkins, F. A. Jr, Crompton, A. W. & Downs, W. R. Mesozoic mammals from Arizona: new evidence on mammalian evolution. *Science* **222**, 1233–1235 (1983).
9. Crompton, A. W. & Jenkins, F. A. Jr. Molar occlusion in Late Triassic mammals. *Biol. Rev. Camb. Philos. Soc.* **43**, 427–458 (1968).
10. Lieberman, D. E. & Crompton, A. W. Why fuse the mandibular symphysis? A comparative analysis. *Am. J. Phys. Anthropol.* **112**, 517–540 (2000).
11. Beecher, R. M. Function and fusion at the mandibular symphysis. *Am. J. Phys. Anthropol.* **47**, 325–335 (1977).
12. Hylander, W. L., Johnson, K. R. & Crompton, A. W. Loading patterns and jaw movements during mastication in *Macaca fascicularis*: a bone-strain, electromyographic, and cineradiographic analysis. *Am. J. Phys. Anthropol.* **72**, 287–314 (1987).
13. Wible, J. R., Rougier, G. W., Novacek, M. J. & Asher, R. J. The eutherian mammal *Maelestes gobiensis* from the Late Cretaceous of Mongolia and the phylogeny of Cretaceous Eutheria. *Bull. Am. Mus. Nat. Hist.* **122**, 1–124 (2009).
14. Beiriger, A. & Sears, K. E. Cellular basis of differential limb growth in postnatal gray short-tailed opossums (*Monodelphis domestica*). *J. Exp. Zool. B* **322**, 221–229 (2014).
15. Crompton, A. W. & Hiiemae, K. M. Molar occlusion and mandibular movements during occlusion in the American opossum, *Didelphis marsupalis*. *Zool. J. Linn. Soc.* **49**, 21–47 (1970).
16. Menegaz, R. A., Baier, D. B., Metzger, K. A., Herring, S. W. & Brainerd, E. L. XROMM analysis of tooth occlusion and temporomandibular joint kinematics during feeding in juvenile miniature pigs. *J. Exp. Biol.* **218**, 2573–2584 (2015).
17. Vandebroek, G. Origin of the cusps and crests of the tribosphenic molar. *J. Dent. Res.* **46**, 796–804 (1967).
18. Hiiemae, K. & Crompton, A. W. in *Functional Vertebrate Morphology* (eds Bramble, D. M. et. al) 262–290 (Harvard Univ. Press, Cambridge, 1985).
19. Mills, J. R. E. A comparison of lateral jaw movements in some mammals from wear facets on the teeth. *Arch. Oral Biol.* **12**, 645–661 (1967).
20. Brainerd, E. L. et al. X-ray reconstruction of moving morphology (XROMM): precision, accuracy and applications in comparative biomechanics research. *J. Exp. Zool. A* **313**, 262–279 (2010).
21. Orsbon, C. P., Gidmark, N. J. & Ross, C. F. Dynamic musculoskeletal functional morphology: integrating diceCT and XROMM. *Anat. Rec. (Hoboken)* **301**, 378–406 (2018).
22. Sánchez-Villagra, M. R. & Smith, K. K. Diversity and evolution of the marsupial mandibular angular process. *J. Mamm. Evol.* **4**, 119–144 (1997).
23. Wible, J. R. On the cranial osteology of the short-tailed opossum *Monodelphis brevicaudata* (Didelphidae, Marsupialia). *Ann. Carnegie Mus.* **72**, 137–202 (2003).
24. Luo, Z. X., Ji, Q., Wible, J. R. & Yuan, C. X. An Early Cretaceous tribosphenic mammal and metatherian evolution. *Science* **302**, 1934–1940 (2003).
25. O'Leary, M. A. et al. The placental mammal ancestor and the post-K–Pg radiation of placentals. *Science* **339**, 662–667 (2013).
26. Luo, Z. X., Yuan, C. X., Meng, Q. J. & Ji, Q. A Jurassic eutherian mammal and divergence of marsupials and placentals. *Nature* **476**, 442–445 (2011).
27. Gatesy, J. & Springer, M. S. Phylogenomic red flags: homology errors and zombie lineages in the evolutionary diversification of placental mammals. *Proc. Natl Acad. Sci. USA* **114**, E9431–E9432 (2017).
28. Grossnickle, D. M. The evolutionary origin of jaw yaw in mammals. *Sci. Rep.* **7**, 45094 (2017).
29. Rowe, T. B. *Osteological Diagnosis of Mammalia, L.1758, and its Relationship to Extinct Synapsida*. PhD thesis, Univ. of California, Berkeley (1986).
30. Rowe, T. Definition, diagnosis, and origin of Mammalia. *J. Vertebr. Paleontol.* **8**, 241–264 (1988).
31. Rowe, T. Coevolution of the mammalian middle ear and neocortex. *Science* **273**, 651–654 (1996).
32. Murray, P. F. A unique jaw mechanism in the echidna, *Tachyglossus aculeatus* (Monotremata). *Aust. J. Zool.* **29**, 1–5 (1981).
33. Luo, Z. X., Cifelli, R. L. & Kielan-Jaworowska, Z. Dual origin of tribosphenic mammals. *Nature* **409**, 53–57 (2001).

Acknowledgements We thank A. Biewener, P. Ramirez and the remaining staff at the Concord Field Station, Harvard University, for their support; S. Gatesy for invaluable advice and assistance with Maya; G. Wagner, J. Maziarz and the rest of the Wagner Laboratory for arranging transfer of the study subjects; K. Zyskowski for assistance in preparing and accessioning specimens; and D. B. Baier for developing the XROMM Maya tools. B.-A.S.B. and J.A.M. were supported by Yale University and the Yale Peabody Museum of Natural History. A.R.M. and E.L.B. were supported by Brown University, by an NSF Graduate Research Fellowship awarded to A.R.M. and by NSF grants 1661129 and 1655756 to E.L.B. E.A.H. was supported by The University of Texas at Austin and by an NSF Graduate Research Fellowship. C.M. and A.W.C. were supported by the Harvard Museum of Comparative Zoology.

Reviewer information *Nature* thanks Anthony Herrel and the other anonymous reviewer(s) for their contribution to the peer review of this work.

Author contributions B.-A.S.B. and A.W.C. conceived and directed the study. J.A.M. performed surgeries with assistance from C.M., A.W.C. and B.-A.S.B. C.M., A.W.C., E.L.B., J.A.M. and B.-A.S.B. recorded trials and performed computed-tomography scans. E.A.H. and B.-A.S.B. segmented and interpreted skeletal and muscular computed tomography data. A.R.M., C.M., B.-A.S.B. and E.L.B. processed videos and generated XROMM data. A.R.M. and B.-A.S.B. prepared figures, and B.-A.S.B. performed morphometric analyses. B.-A.S.B., A.R.M. and E.A.H. wrote the paper.

Competing interests The authors declare no competing interests.

Additional information
Extended data is available for this paper at https://doi.org/10.1038/s41586-019-0940-x.
Supplementary information is available for this paper at https://doi.org/10.1038/s41586-019-0940-x.
Reprints and permissions information is available at http://www.nature.com/reprints.
Correspondence and requests for materials should be addressed to B.-A.S.B.
Publisher's note: Springer Nature remains neutral with regard to jurisdictional claims in published maps and institutional affiliations.

METHODS

No statistical methods were used to predetermine sample size. The experiments were not randomized and investigators were not blinded to allocation during experiments and outcome assessment.

All animal work was performed according to standard protocols approved by the Harvard University (IACUC protocol 14-11-222).

Full methods are provided in the Supplementary Information. For jaw shape comparison, we used the program TPSDig to place nine landmarks, as shown in Extended Data Figs. 1, 2c, on a selection of pan-mammalian jaws, which included a wide array of taxa on the stem of mammals, the stem and crown of monotremes, the stem of theria, and the stems and crowns of marsupials and placentals. We included at least one representative of all marsupial and placental 'orders', selecting taxa in such a way that we captured a mix of apparently conservative and apparently derived mandibular architectures. Landmark placement descriptions were as follow: (1) the anterior intersection of the oral margin and the ventral margin of the dentary; (2) change in the inflection of the ventral margin corresponding to the posterior limit of symphysis; (3) the posterior tip of the angular process (if no angular process was present, the change in inflection at the base of the condylar process); (4) the deepest part of angle between the upper margin of the angular process and the lower margin of the condylar process (if no angular process was present, the halfway point between landmarks 3 and 4); (5) the posterior extreme of the condylar surface (with the oral margin as the anteroposterior axis); (6) the anterior extreme of the condylar surface; (7) the change in inflection between the dorsal and posterior margins of the coronoid process; (8) the dorsal extreme of the coronoid process, with a dorsoventral axis perpendicular to the oral margin; and (9) the intersection of the anterior coronoid margin and the oral margin.

We used the software MorphoJ v.1.06 to perform a full Procrustes fit, generate a covariation matrix and conduct a principal component analysis on the landmark positions. Phylogenetic analyses used a constraint tree assembled in Mesquite v.3.51.

To study the movement of the hemimandibles during mastication, three short-tailed opossums (*M. domestica*; individual 1, 141 g; individual 2, 135 g; individual 3, 144 g) were obtained from Yale University's *Monodelphis* colony and housed in the Animal Facility at Harvard University; all surgical and experimental techniques were approved by Harvard University's Institutional Animal Care and Use Committee. The three individuals were trained to eat in an elevated bin. Feeding was observed in all three opossums before surgery. Marker-implantation surgery and XROMM analysis were performed on individuals 1 and 2.

Food used in trials was either kibble (hard food) or wax worms (soft food). Some size variation is naturally present among kibble pieces and wax worms, which is unfortunate but unavoidable.

Anaesthesia was induced and maintained with isoflurane. Carprofen was administered as an analgesic. Holes were drilled in upper canines and third premolars and lower canines, third premolars, and second molars using a dental drill (Vet Base Silent Surge model EAF2000; Henry Schein), and were filled with radiopaque amalgam. Additionally, one to two 0.5 mm diameter radiopaque tantalum beads (Bal-Tec) were press-fit into hand-drilled holes in the corpus of each hemimandible. See Extended Data Fig. 5a, b for locations of radiopaque markers in both individuals.

We placed the subjects in an elevated bin centred in the X-ray volume created by two X-ray image systems comprising C-arms with 30.6-cm image intensifiers (model 9400; OEC Diasonics, remanufactured by Radiological Imaging Services, 70 kV, 5 mA, magnification level 2) at the Concord Field Station Video Radiography Facility. A total of six biplanar fluoroscopic videos of feeding on wax worms and kibble was recorded (250 fps, 1/500 shutter speed, 1,024× 1,024 resolution) using Photron 1024 PCI video cameras (Photron USA). Still X-ray images of a standard grid and an object of known geometry were also captured to allow the removal of distortion, and the 3D calibration of the cameras[20,34].

Following video data collection, subjects were induced with isoflurane and euthanized using an overdose of sodium pentobarbitol. Subjects were frozen and decapitated, and computed-tomography scans (85 kV, 80 μA, tungsten target, 1-s exposure, 3,200 views, no frame averaging, no ring artefact correction) were taken of the crania and hemimandibles on a Nikon Xtek XT H 225 ST high-resolution μCT scanner at the Harvard Center for Nanoscale Systems. All calibration images, X-ray videos and computed tomography files were uploaded to the XMAPortal, which is a web environment for the storage, management and sharing of XROMM data (http://xmaportal.org/webportal/, under study identifier HARVARD1). Mesh models of skeletal elements and radiopaque markers were reconstructed using VG Studio (version 2.2; Volume Graphics) and cleaned using Geomagic Studio 2013 (3D Systems), in which geometric primitives were fit to the condyles of the hemimandibles and the glenoid fossae of the cranium. Models and primitives were imported into Maya 2016 (Autodesk), and coordinate systems and reference poses were generated as described in the Supplementary Information.

To reconstruct muscle architecture, several frozen male *Monodelphis* specimens were formalin-fixed and stored in alcohol, and then transferred to IKI solution. Staining proceeded with agitation for two weeks, and the resulting preparations were scanned using the same settings above at the Harvard Center for Nanoscale Systems. Muscle attachment sites were identified and marked on models of the cranium and left hemimandible in Maya 2016 (Autodesk). Eight fibres were modelled from the lateral pterygoid, 10 from the medial pterygoid, 15 from the superficial part of the masseter, 15 from the deep part of the masseter, 9 from the superficial part of the temporalis and 16 from the deep part of the temporalis. Mean 'muscle lengths' were then calculated by taking the average of Euclidean distances between attachment sites for each modelled fibre per muscle (see Extended Data Fig. 9).

We developed joint coordinate systems to quantify six-degree-of-freedom kinematics at the temporomandibular joints.

X-ray videos were calibrated and digitized using XMALab v.1.5.0. Rigid-body transformations were computed and filtered using a low-pass Butterworth filter (cut-off frequency: cranium = 20 Hz, hemimandibles = 30 Hz), and then used to animate bone models in Maya, in which six-degree-of-freedom kinematics were calculated from the joint coordinate systems using the 'Output Relative Motion' script in the XROMM_MayaTools package (available at http://xmaportal.org/webportal/).

Reporting summary. Further information on research design is available in the Nature Research Reporting Summary linked to this paper.

Data availability

The raw X-ray and computed-tomography data from the opossums have been deposited in the XMAPortal (http://xmaportal.org/webportal/, with study identifier HARVARD1). Source Data for Figs. 2, 3 and Extended Data Figs. 6–9 are provided with the paper. All other data that support the findings of this study are available from the corresponding author on request.

34. Knörlein, B. J., Baier, D. B., Gatesy, S. M., Laurence-Chasen, J. D. & Brainerd, E. L. Validation of XMALab software for marker-based XROMM. *J. Exp. Biol.* **219**, 3701–3711 (2016).

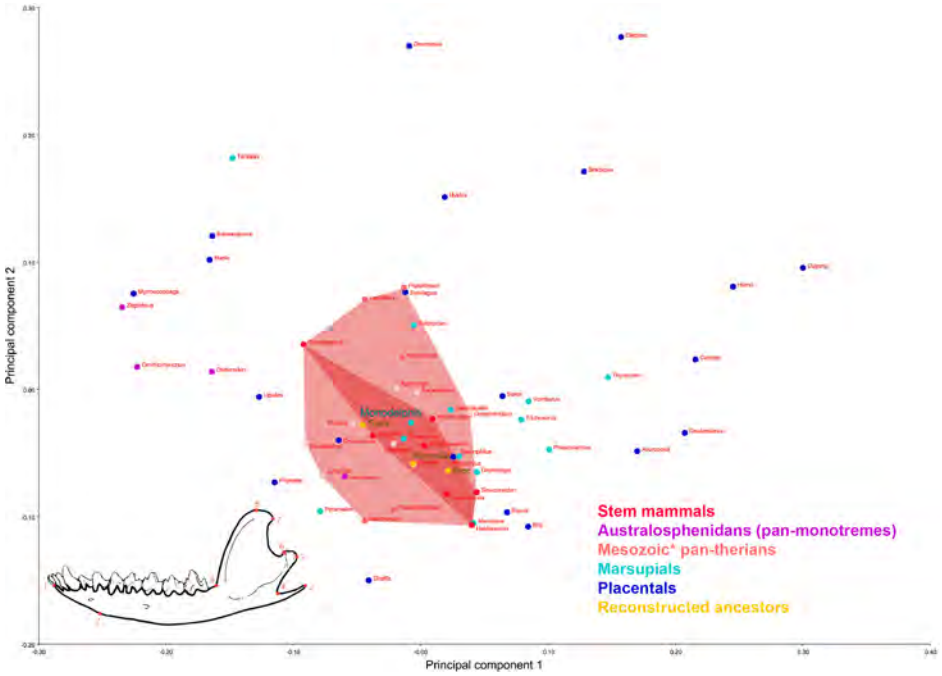

Extended Data Fig. 1 | Geometric morphometric analysis of mammaliaform mandibles, showing the results of principal component analysis of dentary shape. Landmarks on *Monodelphis* dentary, redrawn and modified after ref. [23], are shown in the lower left. The darker red polygon encompasses all stem mammals in the analysis; the lighter red polygon encompasses all Mesozoic mammals and includes all stem therians, stem placentals and stem marsupials. The jaw of *M. domestica* is notably conservative, and falls near the middle of the restricted stem mammal shape-space and the larger stem therian–early therian shape-space. The *M. domestica* jaw is immediately surrounded by the jaws three taxa that are generally considered to be close in form to the mammalian ancestor: *Morganucodon*, *Docodon* and *Hadrocodium*. The 'Mesozoic pan-therians' includes three late-surviving early Cenozoic stem taxa (*Necrolestes*, *Pucadelphys* and *Leptictis*) with ghost lineages that stretch into the Mesozoic; the vertices of the light pink polygon, however, are all confirmed Mesozoic taxa.

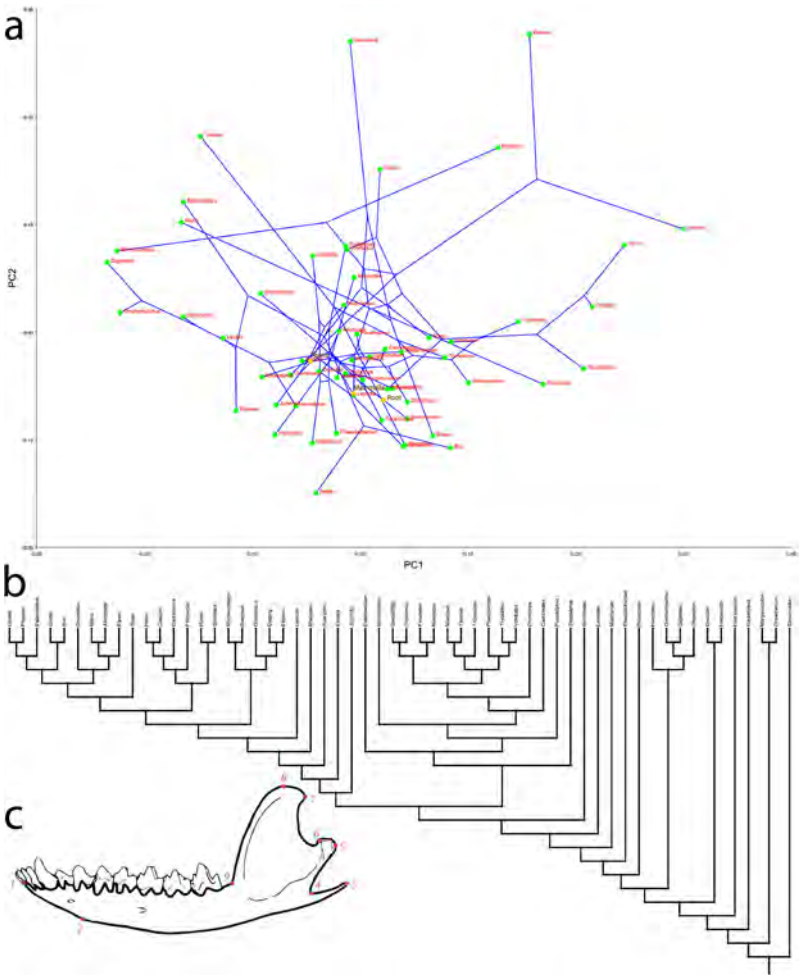

Extended Data Fig. 2 | Phylogenetic framework for geometric morphometric analysis of mammaliaform mandibles. a, Phylogeny, including reconstructed ancestral nodes, superimposed on results from the principal component analysis shown in Extended Data Fig. 1. **b**, Topology used in the analysis, with relationships following previous work[25,28,33]. **c**, Enlarged depiction of landmark positions from Extended Data Fig. 1 upon the *Monodelphis* jaw, redrawn and modified after ref. [23].

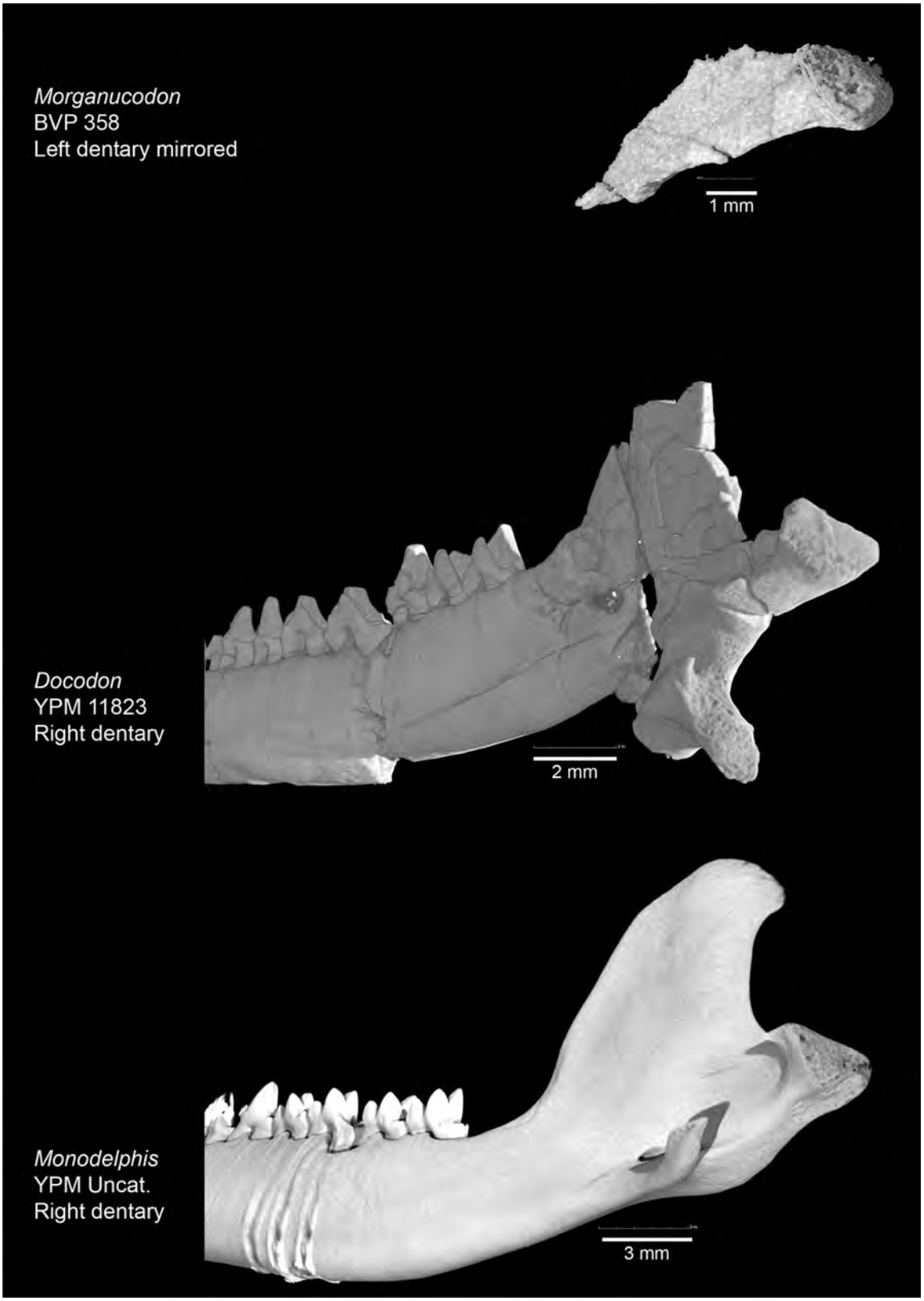

Extended Data Fig. 3 | Condylar regions of mammaliaform dentaries. The dentary condyle of *Monodelphis* is conservative in its orientation, relative size and overall form.

Extended Data Fig. 4 | Typical chewing sequence, shown in anterolateral view. Muscle fibre colours correspond to those in Fig. 1.

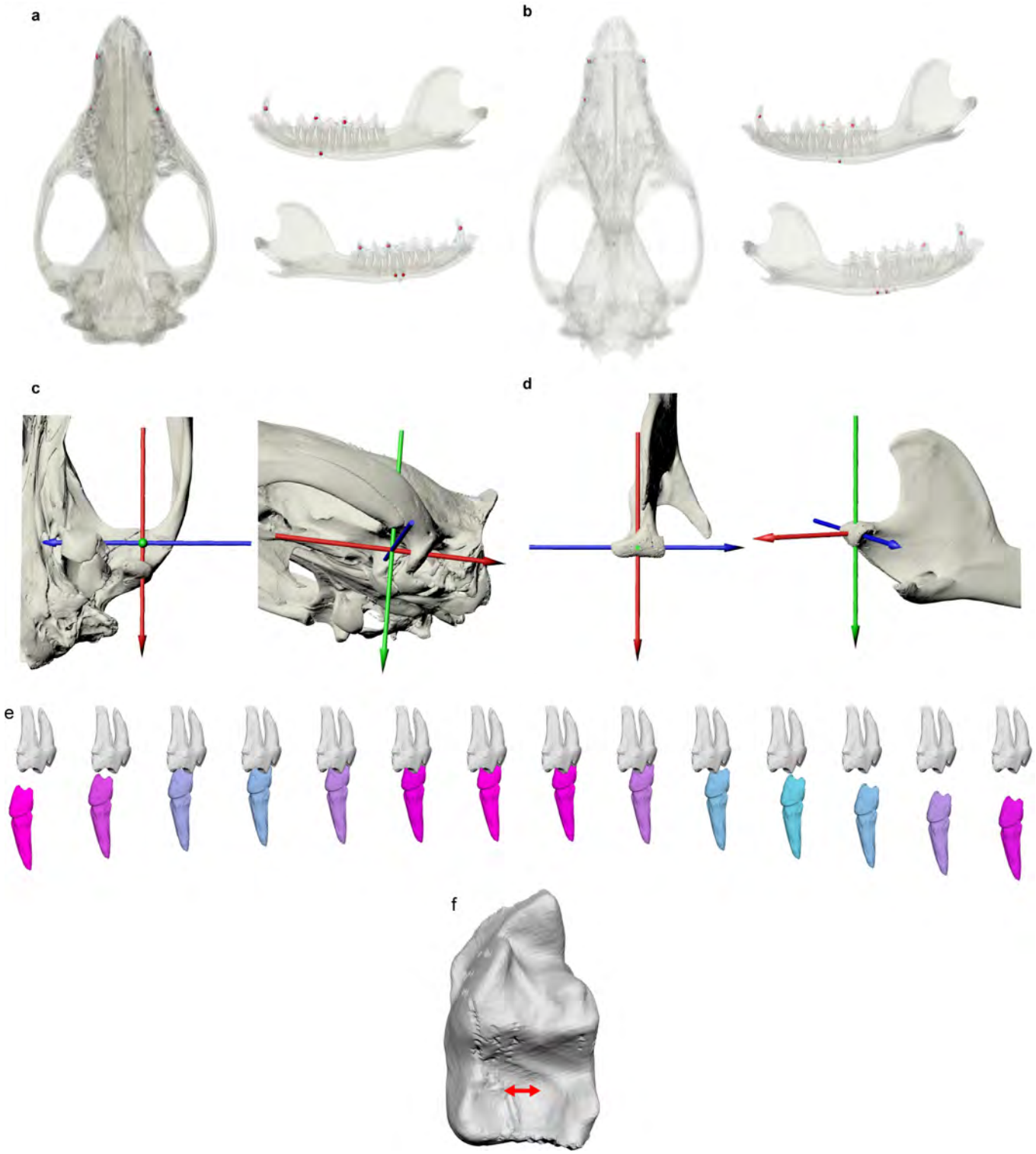

Extended Data Fig. 5 | Marker sites and details of occlusal kinematics. **a**, **b**, Marker implantation sites for individual 1 (**a**) and individual 2 (**b**). Crania in ventral view and hemimandibles in lateral view. **c**, Anatomical coordinate system for the cranium, depicted in ventral and ventrolateral views on the left glenoid fossa of individual 1. **d**, Anatomical coordinate system for the hemimandibles, depicted in dorsal and posteromedial views on the left mandibular condyle of individual 1. **e**, Path of the lower first molar relative to a fixed upper molar; colouring conventions match those in Fig. 3. **f**, Mediolateral distance traversed by the protocone during a power stroke, indicated by red arrows and displayed on the lower first molar of individual 1.

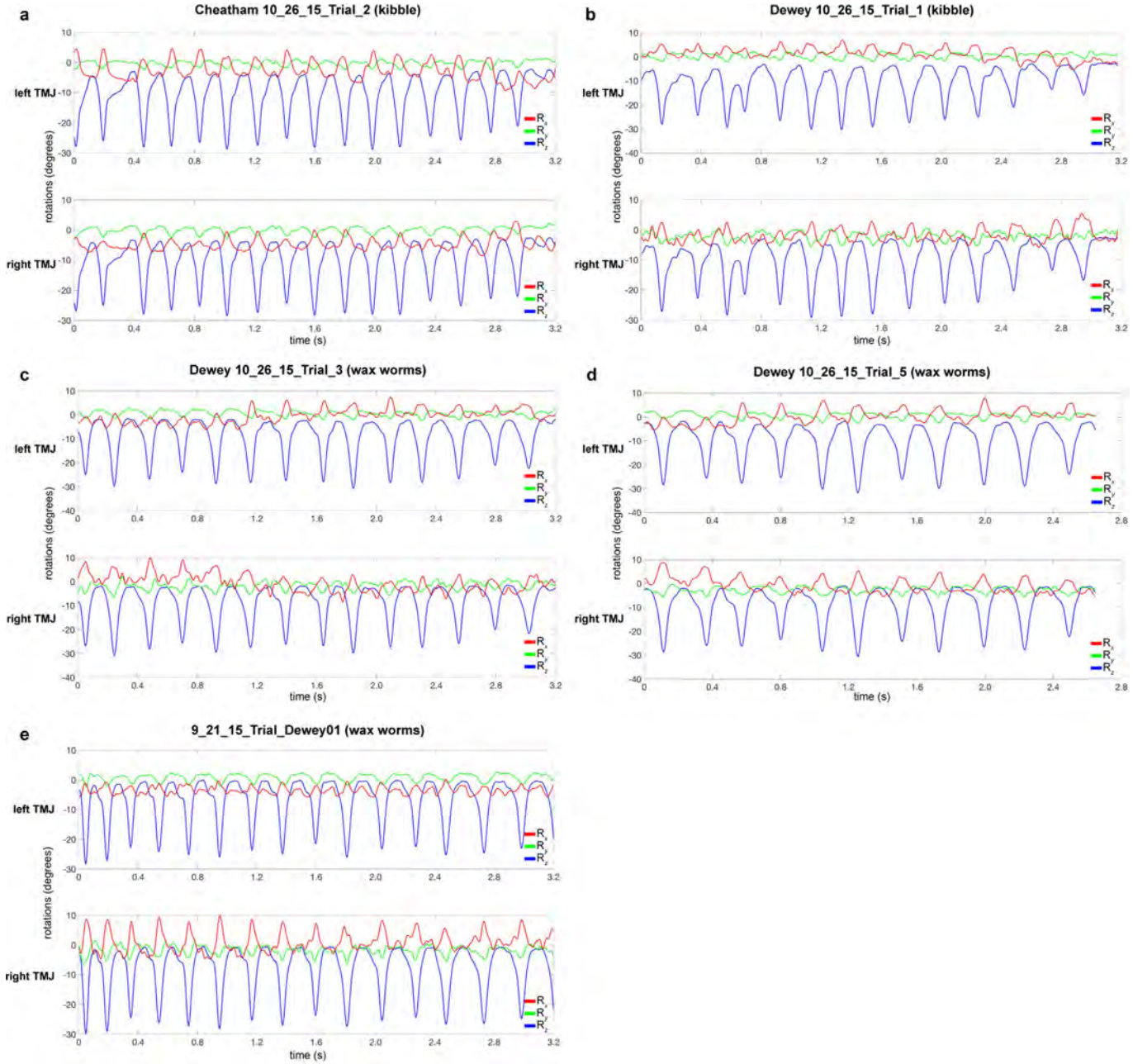

Extended Data Fig. 6 | Temporomandibular joint rotations during five additional trials from two opossums. a, Individual 1 eating kibble. **b**, Individual 2 eating kibble. **c**, Individual 2 eating wax worms. **d**, Individual 2 eating wax worms. **e**, Individual 2 eating wax worms. Titles of the plots match trial names at http://xmaportal.org/webportal/.

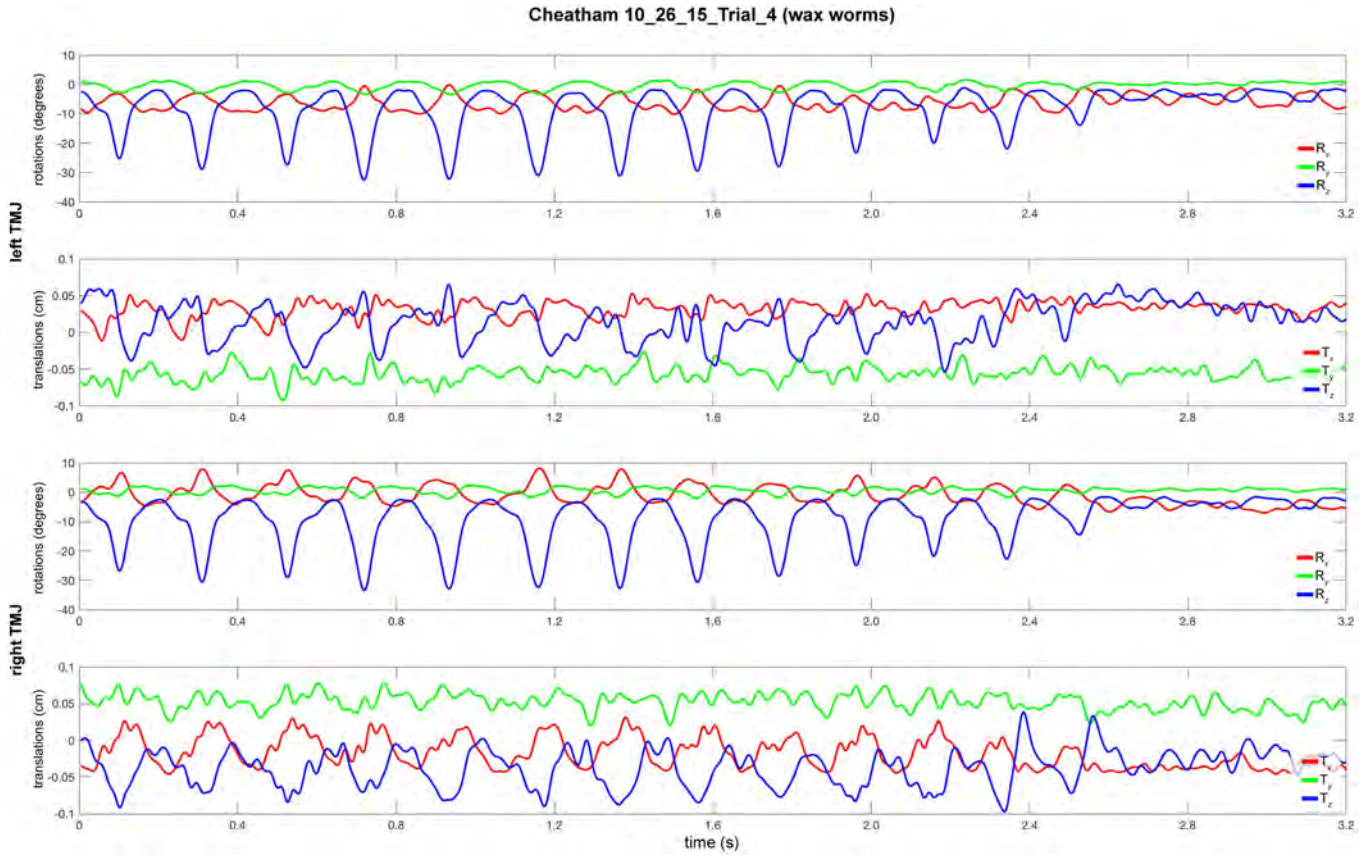

Extended Data Fig. 7 | Left (working side) and right (balancing side) temporomandibular joint rotations and translations for a chewing sequence of individual 1 eating wax worms. Representative of six total trials from two opossums. See 'Description of temporomandibular joint translations' in the Supplementary Information. Title of the plots matches trial name at http://xmaportal.org/webportal/.

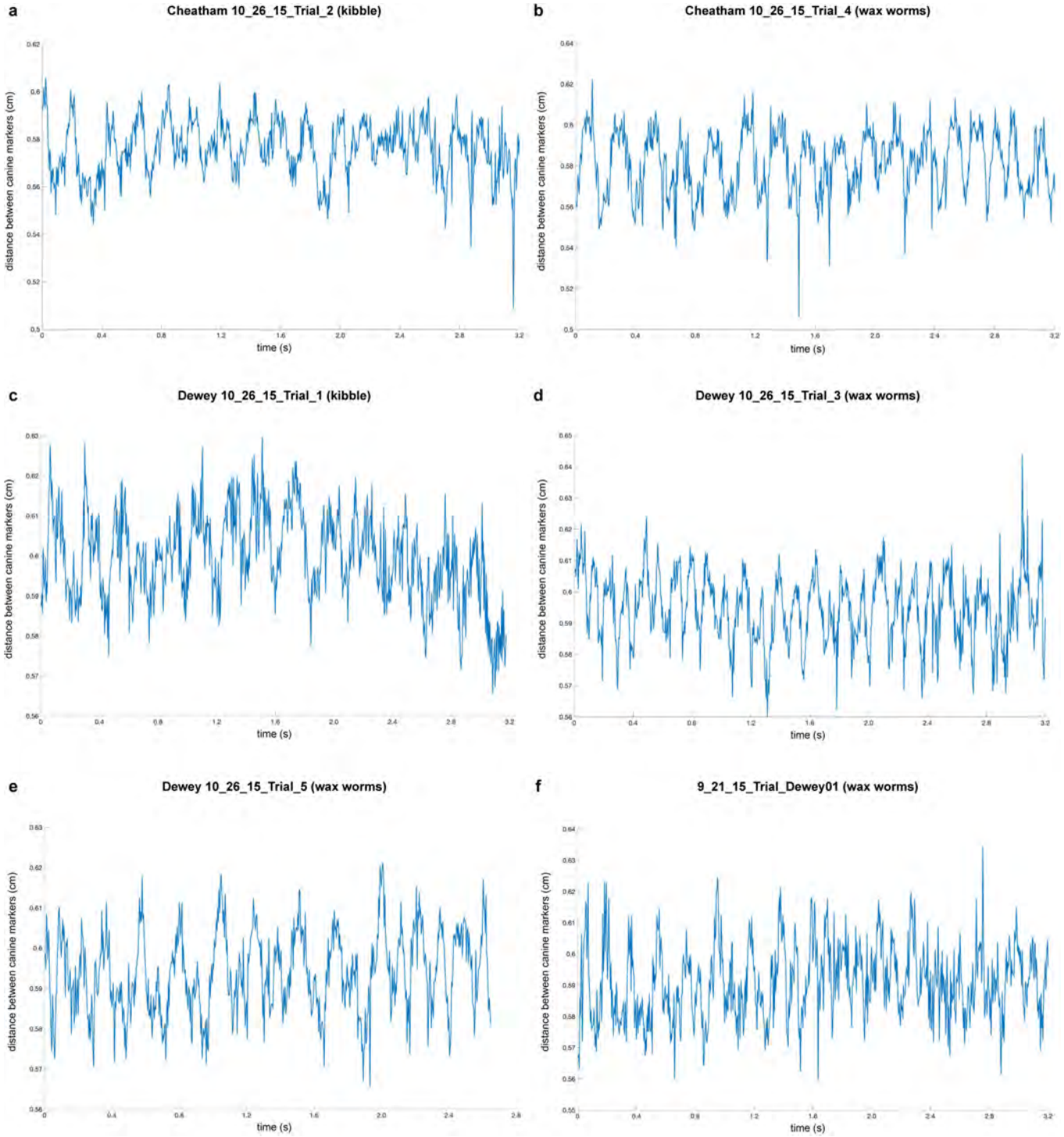

Extended Data Fig. 8 | Distance between radiopaque markers in lower canines during six trials from two opossums, demonstrating the mobility of the mandibular symphysis. a, Individual 1 eating kibble. **b**, Individual 1 eating wax worms. **c**, Individual 2 eating kibble. **d**, Individual 2 eating wax worms. **e**, Individual 2 eating wax worms. **f**, Individual 2 eating wax worms. Titles of plots match trial names at http://xmaportal.org/webportal/.

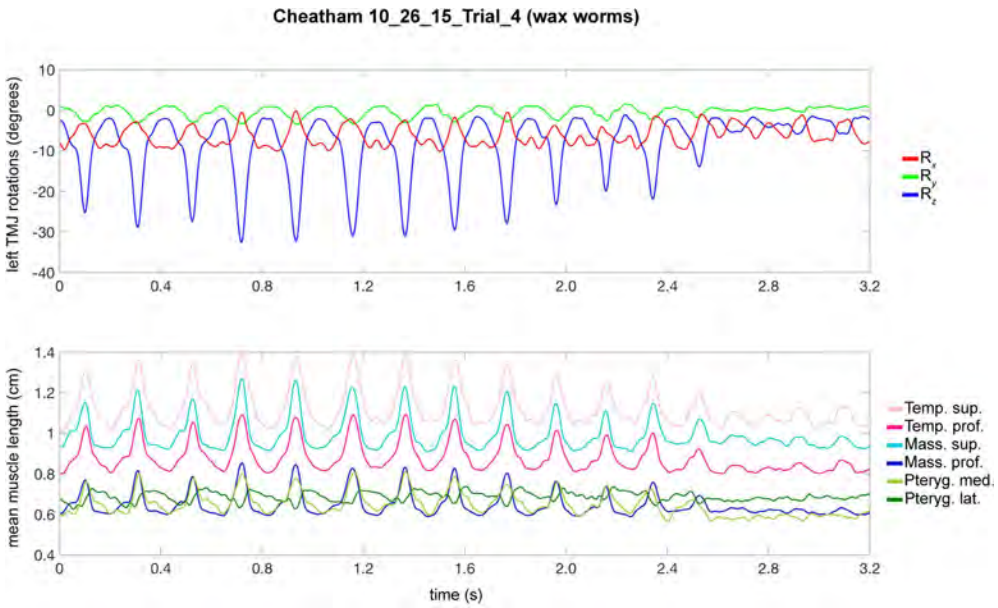

Extended Data Fig. 9 | Left (working side) temporomandibular joint rotations and mean muscle lengths. Euclidean distance between muscle attachment sites as determined on the basis of contrast-enhanced computed-tomography scans (means taken for all fibres modelled per muscle), for a sequence of individual 1 eating wax worms. Representative of two trials from one opossum; muscle fibres were not reconstructed for individual 2. Muscle colours correspond to those in Figs. 1–3. Title of the plots matches trial name at http://xmaportal.org/webportal/.

nature research

Corresponding author(s): Bhart-Anjan S. Bhullar

Last updated by author(s): Dec 20, 2018

Reporting Summary

Nature Research wishes to improve the reproducibility of the work that we publish. This form provides structure for consistency and transparency in reporting. For further information on Nature Research policies, see Authors & Referees and the Editorial Policy Checklist.

Statistics

For all statistical analyses, confirm that the following items are present in the figure legend, table legend, main text, or Methods section.

n/a	Confirmed	
☐	☒	The exact sample size (*n*) for each experimental group/condition, given as a discrete number and unit of measurement
☐	☒	A statement on whether measurements were taken from distinct samples or whether the same sample was measured repeatedly
☐	☒	The statistical test(s) used AND whether they are one- or two-sided *Only common tests should be described solely by name; describe more complex techniques in the Methods section.*
☐	☒	A description of all covariates tested
☐	☒	A description of any assumptions or corrections, such as tests of normality and adjustment for multiple comparisons
☐	☒	A full description of the statistical parameters including central tendency (e.g. means) or other basic estimates (e.g. regression coefficient) AND variation (e.g. standard deviation) or associated estimates of uncertainty (e.g. confidence intervals)
☐	☒	For null hypothesis testing, the test statistic (e.g. *F*, *t*, *r*) with confidence intervals, effect sizes, degrees of freedom and *P* value noted *Give P values as exact values whenever suitable.*
☒	☐	For Bayesian analysis, information on the choice of priors and Markov chain Monte Carlo settings
☒	☐	For hierarchical and complex designs, identification of the appropriate level for tests and full reporting of outcomes
☒	☐	Estimates of effect sizes (e.g. Cohen's *d*, Pearson's *r*), indicating how they were calculated

Our web collection on statistics for biologists contains articles on many of the points above.

Software and code

Policy information about availability of computer code

Data collection	All software for XROMM data collection is available from XMAPortal.org. TPSDIG v2w32 was used to collect geometric morphometric data.
Data analysis	All XROMM software is available from XMAPortal.org. VGStudio Max v2.2, Geomagic Studio 2013, Maya 2016, and MatLab v1.5.0 were used to produce visualizations. Mesquite v3.51 was used to construct a scaffold tree. MorphoJ v1.06 was used to perform morphometric analyses.

For manuscripts utilizing custom algorithms or software that are central to the research but not yet described in published literature, software must be made available to editors/reviewers. We strongly encourage code deposition in a community repository (e.g. GitHub). See the Nature Research guidelines for submitting code & software for further information.

Data

Policy information about availability of data

All manuscripts must include a data availability statement. This statement should provide the following information, where applicable:

- Accession codes, unique identifiers, or web links for publicly available datasets
- A list of figures that have associated raw data
- A description of any restrictions on data availability

The raw opossum X-ray and CT data have been deposited in the XMAPortal (xmaportal.org; Study Identifier HARVARD1). Source data for Figures 3-4 and Extended Data Figures 7-10 have been provided with the paper. All other data supporting the findings of this study are available from the corresponding author on request.

Field-specific reporting

Please select the one below that is the best fit for your research. If you are not sure, read the appropriate sections before making your selection.

☐ Life sciences ☐ Behavioural & social sciences ☒ Ecological, evolutionary & environmental sciences

For a reference copy of the document with all sections, see nature.com/documents/nr-reporting-summary-flat.pdf

Ecological, evolutionary & environmental sciences study design

All studies must disclose on these points even when the disclosure is negative.

Study description	Chewing data from 2 opossum individuals over 6 trials, varying food hardness (hard or soft).
Research sample	3 male Monodelphis, 2 used in experiments.
Sampling strategy	Sample size was chosen on the basis of low variation among individuals documented previously and best practices set by other XROMM studies.
Data collection	Data were collected by authors as detailed in Author Contributions. Primary data recording was conducted by Catherine Musinsky, Alfred W. Crompton, Bhart-Anjan S. Bhullar, Juri A. Miyamae, and Beth Brainerd using a biplanar fluoroscope setup and a microCT scanner.
Timing and spatial scale	Data collected during the spring of 2014 and fall of 2015.
Data exclusions	No data were excluded.
Reproducibility	Repeat experiments and qualitative observations supported our conclusions. Replication consisted of repeated trials with animals on different days. All major findings were successfully replicated.
Randomization	N/A -- no groups used.
Blinding	N/A -- data were collected and processed with minimal interpretation required. No opportunity for blinding.

Did the study involve field work? ☐ Yes ☒ No

Reporting for specific materials, systems and methods

We require information from authors about some types of materials, experimental systems and methods used in many studies. Here, indicate whether each material, system or method listed is relevant to your study. If you are not sure if a list item applies to your research, read the appropriate section before selecting a response.

Materials & experimental systems

n/a	Involved in the study
☒	☐ Antibodies
☒	☐ Eukaryotic cell lines
☒	☐ Palaeontology
☐	☒ Animals and other organisms
☒	☐ Human research participants
☒	☐ Clinical data

Methods

n/a	Involved in the study
☒	☐ ChIP-seq
☒	☐ Flow cytometry
☒	☐ MRI-based neuroimaging

Animals and other organisms

Policy information about studies involving animals; ARRIVE guidelines recommended for reporting animal research

Laboratory animals	Short-tailed opossum Monodelphis domestica; 3 male individuals
Wild animals	N/A
Field-collected samples	N/A
Ethics oversight	Harvard University IACUC and animal resources staff

Note that full information on the approval of the study protocol must also be provided in the manuscript.